ACS OMEGA

Open Access

http://pubs.acs.org/journal/acsodf

Article

Intriguing and Facile Preparation Approach of CdO Nanorod-Based Abundant Chitosan for Symmetric Supercapacitors

Rania A. Elmanfaloty, Kamel R. Shoueir,* and Bedir Yousif

Cite This: *ACS Omega* 2023, 8, 35682−35692

Read Online

ACCESS | Metrics & More | Article Recommendations

ABSTRACT: Abundant chitosan was rationally used for the green fabrication of cadmium oxide nanorods (CdO nanorods) owing to its environmentally benign characteristics, bioavailability, low cost, etc. However, the primary unsubstituted amino group of chitosan interacts with the surface of Cd salt at higher temperatures, resulting in CdO nanorod formation. A one-step hydrothermal technique was adopted in the presence of chitosan. Optical, structural, and morphology techniques characterized CdO nanorods. According to X-ray diffraction crystallography, CdO is well crystallized in the face-centered cubic lattice with an *Fm*-3*m* (225) space group. The AC@CdO nanoelectrode demonstrated an outstanding gravimetric capacitance of 320 F g^{-1} at a current density of 0.5 A g^{-1}, nearly three-fold that of ordinary AC electrodes. The AC electrode and the AC@CdO nanoelectrode retain 90 and 93% of their initial specific capacitance after 10,000 galvanostatic charge discharge cycles. The AC@CdO nanoelectrode has a lower equivalent series resistance value than the AC electrode. Moreover, AC@CdO symmetric supercapacitor devices achieve excellent results in terms of specific energy, specific power, and capacitance retention.

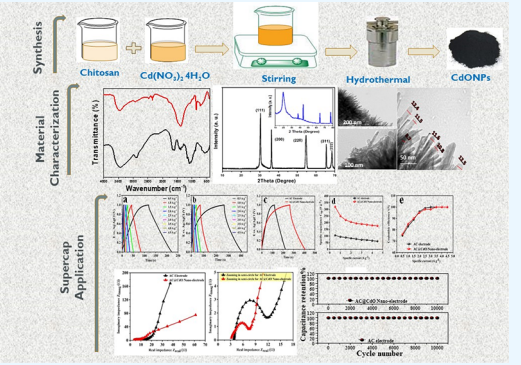

1. INTRODUCTION

Recently, the rapidly expanding economic growth, rising environmental pollution, and the use of fossil fuels are all critical issues for humanity, necessitating the urgent need for alternative energy sources and storage energy transformation.[1,2] Electrochemical energy storage (EES), also known as supercapacitors, has emerged as an innovative method of storing energy conversion.[3] Since it has extended cycle stability, fast charge−discharge flux, and high power density, it is ideal for high-power uses; the EES system has played a critical role in the development of energy storage devices enabling upcoming portable electronic gadget technologies, hybrid electric autos, and all-electric vehicles.[4,5] Supercapacitors in an electrochemical system are categorized into electric double-layer capacitors (EDLCs) and electrochemical pseudocapacitors (EPCs). However, EDLCs cannot replace more conventional battery technologies because of their low energy density.[6]

Pseudocapacitors have higher electrochemical activity, increasing energy density, and capacitance.[7] False capacitors have a lower power density and shorter cycle life.[8] Asymmetric supercapacitors, also termed supercapattery devices, combine the advantages of EDLCs and pseudocapacitors to overcome their drawbacks. In function and performance, it's like a battery-supercapacitor hybrid. Compared to standalone supercapacitors and battery systems, this hybrid system's energy and power densities are notable, placing it in the category of excellent energy storage.[9] Better storage properties of supercapattery devices are heavily dependent on electrode fabrication procedures.

Metallic nanostructures, MOFs, phosphides, layered double hydroxides, and carbon-based compounds are all choices for electrode composition.[10] Hydro/solvothermal synthesis, sol−gel, co-precipitation, green synthesis, etc., are being discussed to create nanoparticles.[11] In this regard, nanoparticles can be synthesized utilizing various old processes that are expensive, hazardous, and harmful to the environment.[12] Chemical synthesis methodologies for nanoparticles include electrochemical methods,[13] sonochemical,[14] and chemical reduction.[15] Mechanical procedures include grinding, milling, sputtering, and physical processes such as thermal/laser ablation.[16] These nanoparticle preparation approaches each have merits and limitations.[17]

In light of the desire for sustainable development, the green synthetic approach of creating nanoparticles has dramatically increased in relevance.[1] Most synthesis procedures are

Received: April 4, 2023
Accepted: August 31, 2023
Published: September 18, 2023

dangerous due to the chemical compositions they exploit, meaning they may not serve the objective of sustainable development as envisaged.[18] As an added downside, such procedures frequently involve potential harm and chemical exposure. Therefore, sustainable development aims can be efficiently accomplished by creating and developing harmless chemical ways of manufacturing electrode materials, known as green synthesis.[19] Green synthesis, which uses plant extraction, is seen as particularly promising among the several existing technologies thanks to benefits like its nontoxic nature and low cost. No excessive heat, pressure, or energy is required during synthesis.[20] Otherwise, algae, fungi, bacteria, and polymers can all participate in this eco-friendly synthesis.[21]

Chitin is a polysaccharide extracted by deacetylation to yield chitosan.[22] Chitin is derived from the exoskeleton of crustaceans like shrimp, crabs, and lobsters.[23] It shows promise as a tissue engineering material for treating hypertension, promoting wound recovery, and aiding in supercapacitance investigation.[24−27] Chitosan has remarkable synergistic effects when combined with metals, metal oxide nanoparticles, and polymers. The surface features of the nanometal oxides prepared using chitosan as templates have been altered, making them more useful in various applications.[28] Chitosan acts as a template to encourage the development of particles around 100 nm in size to be monodispersed by promoting spatial separation of the particles.[29] Chitosan-based metallic (oxide) nanoparticles, such as chitosan-CuO,[30] chitosan-ZnO,[31] and chitosan-NiO,[29,32] have been the subject of increasing attention in recent years for their potential energy applications.

Several different forms of nanocomposites of transition metal oxides are being employed as electrode materials to accomplish the desired characteristics of a supercapacitor device, as reported in the literature.[17,27,33] Cadmium oxide (CdO) is a transition metal oxide often found in atypical crystalline forms, such as brown or red crystals or a white amorphous powder. CdO is a superb active material for supercap due to its inexpensive cost and inherent dopability, resulting in high electrical conductivity. CdO is considered an n-type semiconductor with an index of refraction of 2.49 with direct and indirect band gap values of 2.3 and 1.36 eV.[34] Only a few studies have been published on CdO alone as an electrode for supercapacitors.[35]

The current investigation offers an eco-friendly using a polymeric biosynthetic technique to develop CdO nanorods with tunable sizes for supercap applications. Chitosan is a cheap, stable, eco-friendly, water-soluble substance serving as a capping, stabilizing, and reducing agent during nanoparticle biosynthesis. Once the CdO was synthesized, the structural and morphological properties were examined using transmission electron microscopy (TEM), scanning electron microscopy (SEM), X-ray diffraction (XRD), etc. Cyclic voltammetry (CV), galvanostatic charge discharge (GCD), and electrochemical impedance spectroscopy (EIS) studied the electrochemical nature of the produced CdO nanoparticles using an electrolyte (KOH).

2. MATERIALS AND METHODS

Deacetylated chitin, poly(D-glucosamine), chitosan (Low M_W) extra pure, 10−150 m. Pa s, 90% DA, supported by Sisco Research Laboratories Pvt. Ltd. India, NMP, *N*-methyl-2-pyrrolidone C_5H_9NO 99.13 g/mol ≥99.5% from MERCK. Cadmium nitrate tetrahydrate, 98%, $Cd(NO_3)_2{\cdot}4H_2O$, synthetic graphite powder, <20 μm, and polyvinylidene fluoride (PVDF), average $M_w \sim 180{,}000$ by GPC, average $M_n \sim 71{,}000$ were purchased from Sigma. Other nonmentioned reagents and solvents were used as received.

2.1. Synthesis of Cadmium Oxide Nanorods (CdO Nanorods) Based on Chitosan. CdONPs were successfully synthesized using $Cd(NO_3)_2{\cdot}4H_2O$, NaOH, and chitosan. The process was quick, easy, and allowed for precise control of the particle size. The diluted acetic acid solution (CH_3COOH) dissolved a fine powder of 0.5 g chitosan to exhibit 0.5 wt %. Next, the mixture was stirred for 20 min after adding 0.1 M NaOH. Subsequently, a specific quantity of 0.2 mol $Cd(NO_3)_2{\cdot}4H_2O$ was gradually incorporated into the 50 mL solution, and the stirring process was sustained for an additional 30 min. The whole reaction was transferred to hydrothermal synthesis autoclave reactor 5 MPa 220C-304 St. St high-pressure (BAOSHISHAN 200 mL) and lasted for 2 h at 180 °C. A brown suspension was formed, which precipitated by centrifugation. After being rinsed multiple times with ethanol, the remaining substance was left to dry overnight at 70 °C.

2.2. Material Characterization. *2.2.1. UV−Vis Spectra.* A double-beam spectrophotometer measured the CdONPs absorbance peak (Bio Aquarius CE 7250, UK). 400 L of CdONPs in water was suspended in 2 mL of Milli-Q water.

2.2.2. TEM. The CdONP suspension was sonicated for 5 min before being precipitated on the carbon-coated grid to bolster the sample and then allowed to be air-dried before analysis. A high-resolution TEM (JEOL, 2100) was used for this purpose at 200 kV.

2.2.3. SEM. An FESEM (model: QUANTA-FEG250, the Netherlands) was used to identify the prepared sample morphology.

2.2.4. XRD. The structural analysis was accomplished by Pertpro (Cu kα1 radiation with λ = 1.5404 Å, 45 kV, 40 mA, USA diffractometer). The XRD pattern was recorded for all compositions.

2.2.5. FTIR. An FTIR spectrometer (Perkin-Elmer 2000) was enrolled to determine the cohesion of the surface's chemical structures of CdONPs, and the research infrared spectra varied from 4000 to 4000 cm^{-1}.

2.2.6. XPS. The powder was examined using the X-ray photoelectron spectroscopy instrument (PerkinElmer PHI 5600). The analysis range was up to 1400 eV with 0.1 eV resolution.

2.3. Preparation of the AC@CdO Nanoelectrode. The current collector nickel sheet was pretreated sequentially with 3 mL of concentrated hydrochloric acid for 0.5 h, washed several times with deionized water, and left to be air-dried for enough time to ensure a clean surface. To fabricate the AC@CdO as a working electrode, then, the homogeneous slurry was applied to the nickel sheet. It was made by combining 46% activated carbon material (AC), 34% cadmium oxide (CdO), 10% carbon black (CB) acetylene, and 10% PVDF in 0.3 mL of NMP as the solvent. The AC@CdO nanoelectrode with a square area of (1 × 1 cm^2) on the current collector was then dried for 12 h at 85 °C in a hot air oven. The fabricated electrode material's mass was estimated to be 3 mg.

2.4. Electrochemical Measurements. With the three-electrode assembly of the working electrode (AC@CdO), CV, GCD, and EIS techniques were applied in an aqueous electrolyte of sodium sulfate (Na_2SO_4). Platinum wire was used as the counter electrode, Ag/AgCl (KCl saturated) as a

https://doi.org/10.1021/acsomega.3c02261
ACS Omega 2023, 8, 35682−35692

reference electrode, and an AC@CdO nanomaterial as a working electrode. At varied scan rates, from 10 to 100 mV s^{-1}, the cyclic voltammograms were recorded in the potential range of 0−1 V. GCD investigations were conducted at various specific currents (0.5 to 4.5 A g^{-1}). Additionally, with a 10 mV amplitude, the EIS was recorded in the frequency range of 100 kHz to 10 MHz.

The explicit capacitance (C_{sp}, F g^{-1}), the specific energy (SE, Wh kg^{-1}), and specific power (SP, W kg^{-1}) were computed based on information gathered from the GCD and CV calculations, and coulombic efficiency (η %) was measured as published earlier.[2,36,37]

3. RESULTS AND DISCUSSION

Chitosan has a strong affinity for metal ions via chelation or an ion exchange pathway, which aids in the nucleation and stability of metal oxide nanoparticles.[22,38] Several research groups have claimed success in using chitosan as a mild reducing and stabilizing agent in the production of metal oxide, demonstrating the latter's antibacterial and catalytic properties.[39] Here, the presence of NaOH participates in the coexistence of elementary CdO and $Cd(OH)_2$.[40] Heating the mixture to more than 100 °C using NaOH as a catalyst in the presence of chitosan is essential in reducing Cd salt to CdO nanorods. The particular interactions between the primary unsubstituted $-NH_2$ of chitosan and the surface of Cd-salt with increasing temperature imply an increase in CdO nanorod

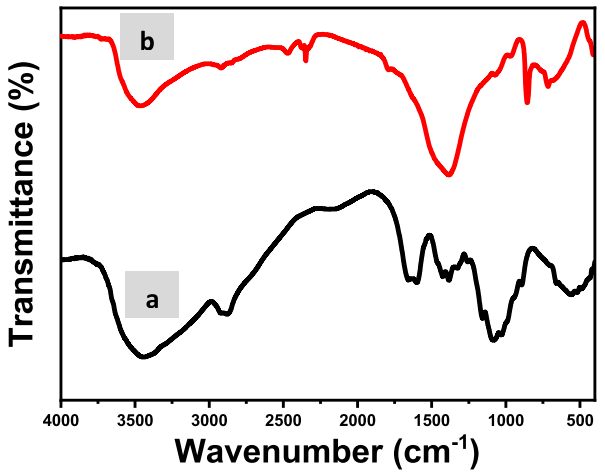

Figure 1. FTIR spectra of (a) chitosan and (b) CdO nanorods.

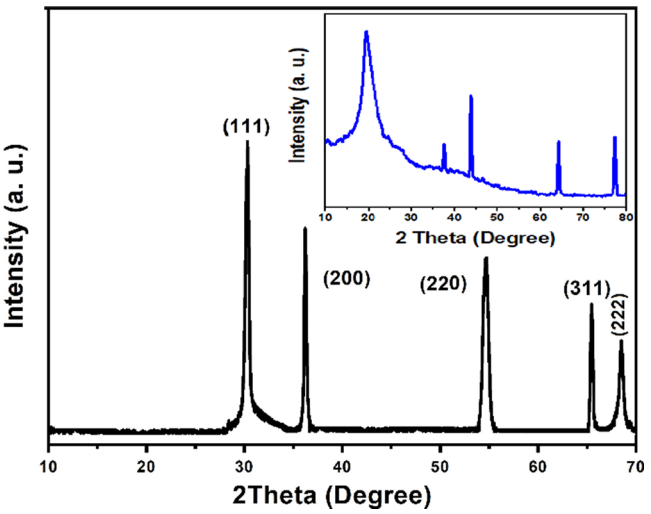

Figure 3. XRD diffractogram of CdO nanorods (inside XRD of pure chitosan).

Table 1. CdO Nanorod X-ray Diffraction Pattern Illustrating Crystallite Sizes Determined via Reflections from 5 (*hkl*) Planes

CdO (*hkl*)	2θ	FWHM	*D* (nm) CdO	average *D* by XRD	average *D* by TEM
(111)	32.183	0.100	36.028	12.80	11.25
(200)	37.540	0.187	6.915		
(220)	55.936	0.216	9.834		
(311)	66.160	0.252	5.6510		
(222)	68.255	0.213	5.588		

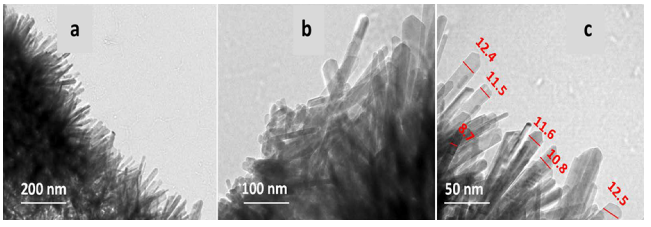

Figure 4. TEM for detection of the shape and size of CdO nanorods: (a) 200 nm scale bar, (b) 100 nm scale bar, and (c) 50 nm scale bar.

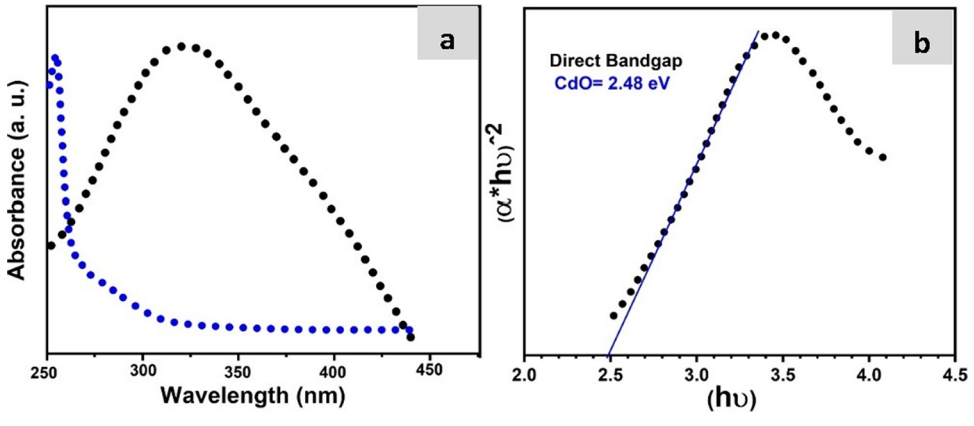

Figure 2. UV of (a) chitosan/CdO nanorods and (b) bandgap calculation of CdONPs.

https://doi.org/10.1021/acsomega.3c02261
ACS Omega 2023, 8, 35682−35692

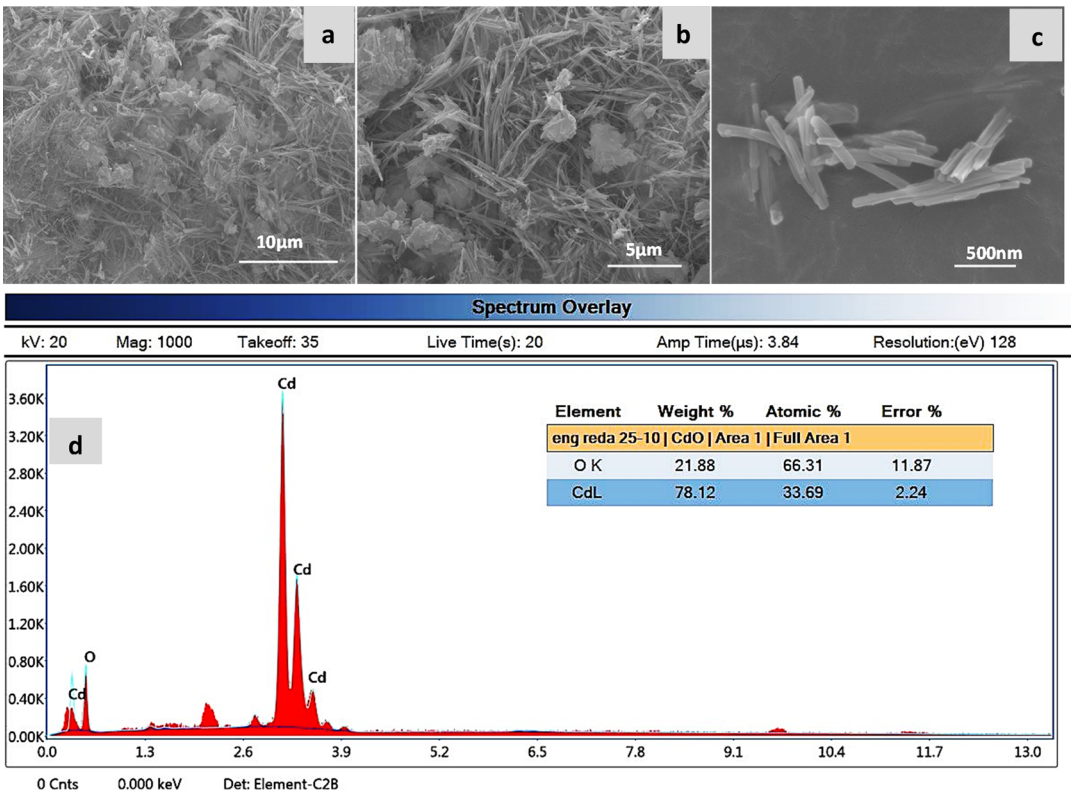

Figure 5. SEM texture of CdO nanorods (a) 10 μm, (b) 5 μm, (c) 500 nm, and (d) EDX spectra.

formation. Autoclave pressure raises the temperature above the boiling point of the solvent medium (water), increasing the energy of the water molecule.[41] When the energy of a system is increased, the average kinetic energy increases; consequently, the particles move faster, resulting in enormous collision energy. The collision of one atom with the existing nucleus is a dominant process in forming a stable nucleus.[42] This may explain why our pressure-assisted system favors growth over nucleation.

3.1. FTIR Spectra. The FTIR spectrum was used to investigate the modes of vibration of chemical bonds present in CdO nanorods prepared by chitosan, and functional groups were recorded in the 400−4000 cm^{-1} range. The FTIR spectrum of CdO nanorods and the distinctive absorption peaks of chitosan are depicted in Figure 1. The peak at 3472 cm^{-1} corresponds to the merged maxima stretching of the $-NH_2$ and −OH moiety vibrations of chitosan.[43] Figure 1b illustrates CdO nanorods that, compared to chitosan, the mighty broader peak migrated to a lesser wave number at 3472 cm^{-1}, confirming a substantial connection between CdO and these groups.[44] Chitosan asymmetric stretching of CH_3 and CH_2 is responsible for the absorption peaks at 2920 and 2858 cm^{-1}. While the absorption peaks at 1791 and 1074 cm^{-1} are attributed to the bending vibration stretching of −NH and C−O groups, new absorption peaks at 714 and 674 cm^{-1} are attributed to the attachment of the −CO−NH group and the stretching mode of CdO.[34,45] Additionally, the distinctive peaks in Figure 1b have been relocated to a lesser wavenumber at a 3472 cm^{-1} wide peak that corresponds to −OH, $-NH_2$, and −CO−NH moieties, moving discernibly and becoming more robust and broader, indicating the potent interaction between CdO with these groups.

3.2. UV−Vis Spectroscopy. Utilizing UV−vis spectroscopy to locate the absorption peak (Figure 2) facilitates a straightforward investigation of the optical properties of metal oxide nanoparticles and polymers. The UV−vis principle states that the atom's outer electrons can be moved to a higher energy level after absorbing radiant energy. The spectrum, including the chitosan and CdO nanorods, band-gap energy, which the adsorption of radiant radiation may capture. The extinction coefficients for wavelengths below 220 nm for ordinary chitosan are due to its transparency.[46] The UV−vis spectrum of the CdO nanorods was shifted, and the spectral changes around 319.5 nm were obtained, depicting that chitosan supports the surface modifications of CdO nanorods and matches with other findings.[47] The band-gap energy of the CdO nanorods was determined using Tauc's rule (direct band-gap rule, γ), and the plot of $\alpha h\gamma^2$ versus $h\gamma$ was extrapolated to the x-axis following the maximization of the absorption level. The band-gap energy for CdO nanorods was determined to be 2.48 eV using the extrapolated curve.

3.3. XRD Diffractogram. The XRD pattern elucidates the as-prepared CdO nanorod and pure chitosan crystal structures (Figure 3). Pure CdONPs, including chitosan, revealed the existence of potential peaks 2θ values at 32.2° (111), 37.8° (200), 55.7° (220), 66.5.0° (311), and 68.4° (222) reticular orientations of the single phase cubic Monteponite CdO structure which also matched with Joint committee on powder diffraction standards (JCPDS card no. 05-0640).[48] The XRD pattern of chitosan alone displayed different peaks; however, the intensity of the most common one around 20° was diminished, and other peaks are decreasing, suggesting that chitosan stabilized CdO nanorods. CdO is well crystallized in the face-centered cubic lattice with an Fm-3m (225) space

https://doi.org/10.1021/acsomega.3c02261
ACS Omega 2023, 8, 35682−35692

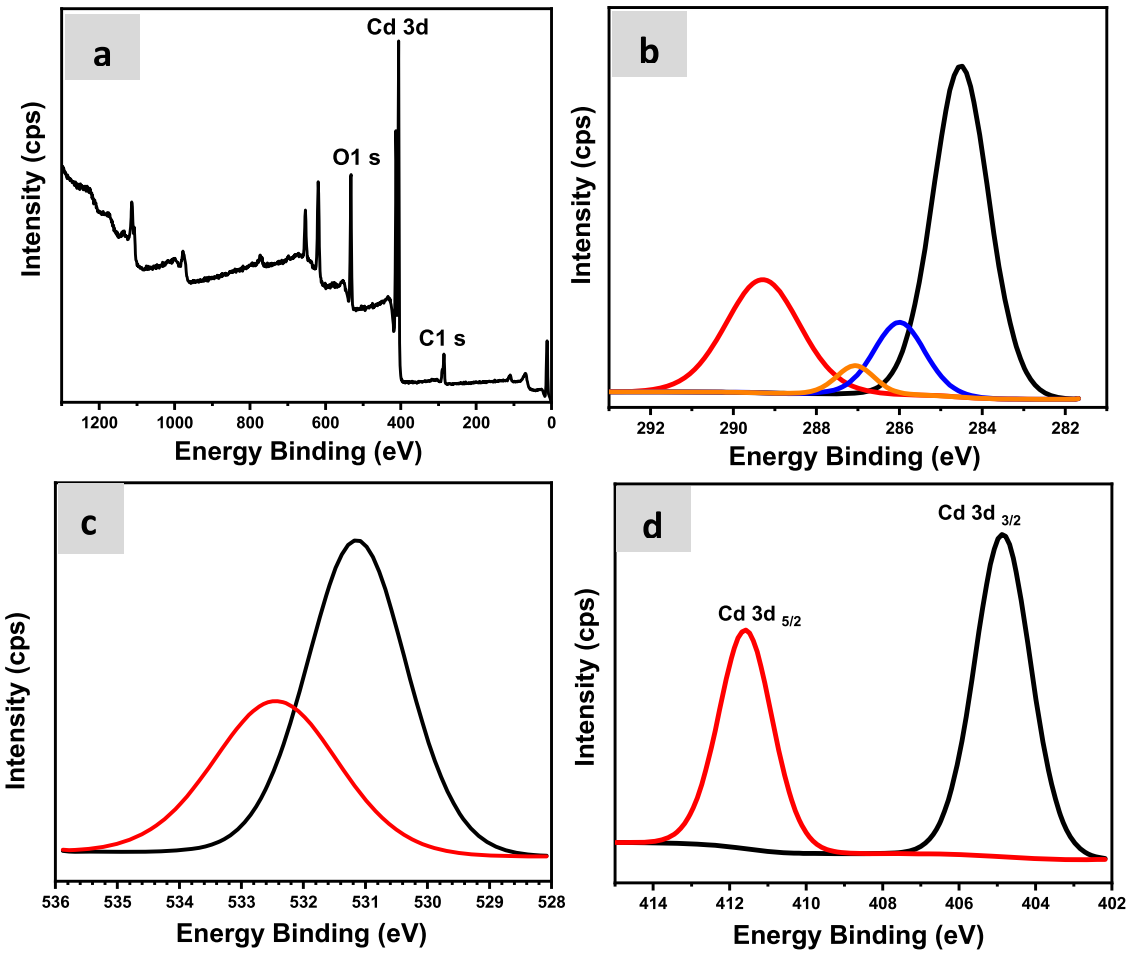

Figure 6. XPS spectra of (a) full spectrum, (b) C 1s, (c) O 1s level, and (d) Cd (3d) spin-orbit components.

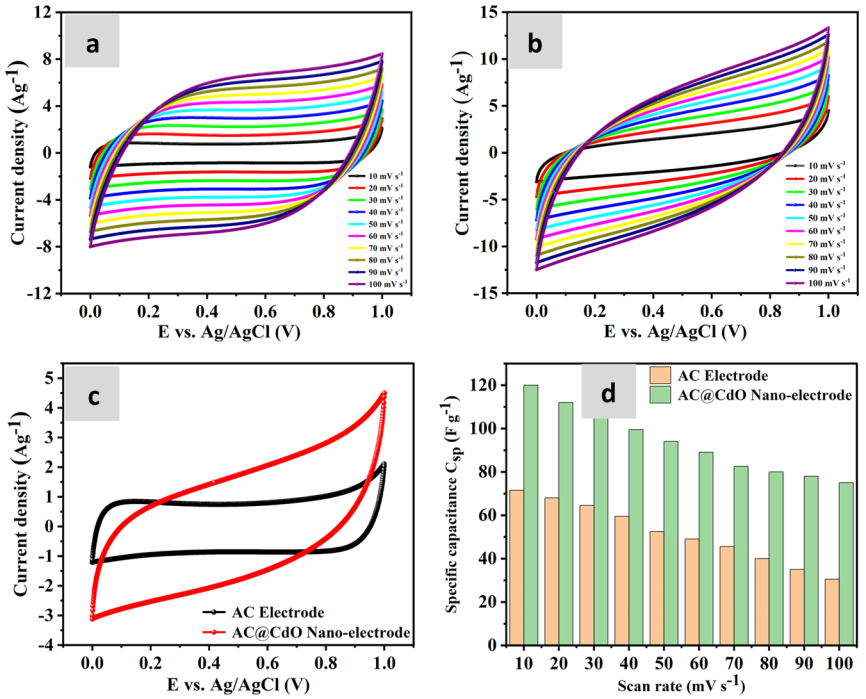

Figure 7. CV curves (a) AC electrode, (b) AC@CdO nanoelectrode at various scan rates, (c) AC electrode and AC@CdO nanoelectrode at a scan rate of 10 mV s^{-1}, and (d) C_{sp} of the AC electrode and AC@CdO nano-electrode.

https://doi.org/10.1021/acsomega.3c02261
ACS Omega 2023, 8, 35682−35692

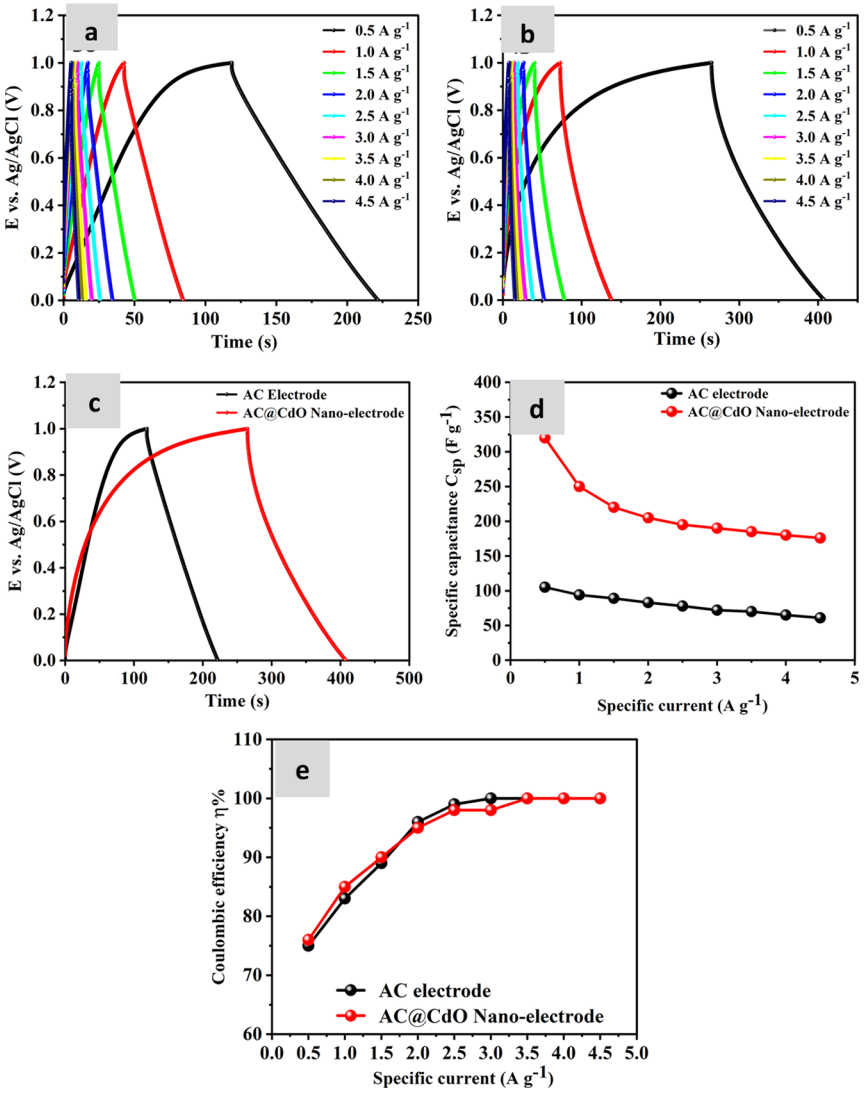

Figure 8. GCD of the (a) ordinary electrode, (b) nanoelectrode, (c) GCD under a current density of 0.5 A g^{-1} for both electrodes, and (d) computed $C_{sp,}$ and (e) η%.

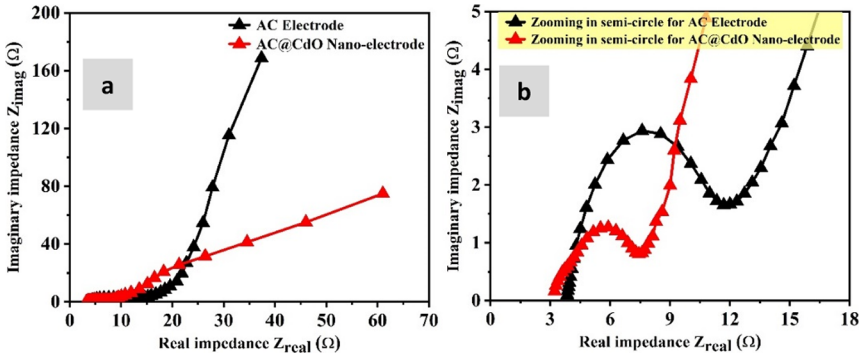

Figure 9. (a) Nyquist plots and (b) semi-circle Nyquist plots using 1 M Na_2SO_4 electrolyte.

Table 2. Characterization Factor for the AC Electrode and AC@CdO Nanomaterial Electrode with 1 M Na_2SO_4 Aqueous Electrolyte @ Potential Window from 0−1 V

electrode	C_{CV} (F g^{-1})	C_{GCD} (F g^{-1})	SE (Wh kg^{-1})	SP (W kg^{-1})	ESR (Ω)	retention%
AC electrode	71.5	105	14.6	510.3	3.9	100
AC@CdO electrode	120	320	44.45	1119	3.05	100

https://doi.org/10.1021/acsomega.3c02261
ACS Omega 2023, 8, 35682−35692

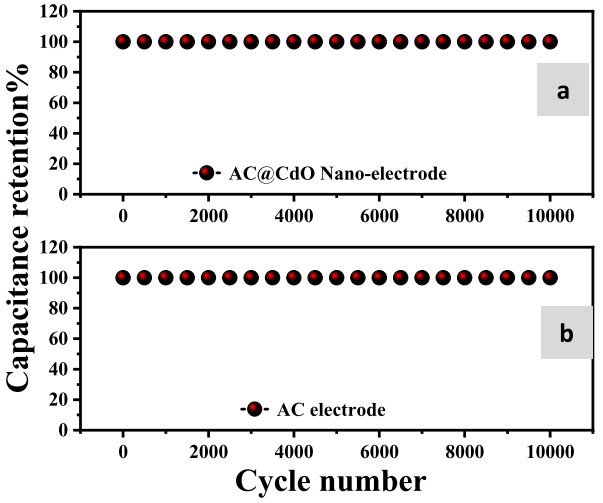

Figure 10. Cycling stability over 10,000 GCD cycles for (a) nanoelectrode and (b) for AC electrode.

group. The crystalline size (D) of CdO nanorods was detected based on the Scherrer equation:

$$D = 0.94\frac{\lambda}{\beta\cos\theta} \quad (1)$$

where λ, X-ray wavelength; θ, Bragg's diffraction angle; and β, FWHM (full width at half-maximum). The value of average size D (nm) calculated from XRD was 12.80 nm and that obtained by TEM was 11.25 nm (Table 1).

3.4. TEM Morphology. Figure 4 depicts TEM pictures of the generated CdO nanorods with an average diameter of 11.25 nm. It agrees well with diameter values obtained from XRD readings. Chitosan solution was employed as a stabilizer in this research to create anisotropically well-defined CdO nanorods. The correct quantity of chitosan solution addition aids in controlling the precipitation operating variables of the required size and shape.[49] Stabilizing ingredient adsorption on appropriate crystal aspects is expected to impact the intrinsic anisotropy in CdO nanostructures. As a result, the expansion rate in the longitudinal orientation is more rapid. It has been documented that transition metal nanocrystals can be easily regulated using a stabilizing reagent, which stops the nanostructures from growing and agglomerating uncontrollably.[50] The nucleation process generally controls the shape and size of nanostructures. Throughout the synthesis, nuclei are generated by self-nucleation with a constant supply of atoms given by precursor breakdown. The generated nuclei will immediately begin to develop in the form of nanocrystals. The form of nuclei has a significant impact on the ultimate nanostructure morphology. Because of the high monomer concentration, the surroundings have a strong chemical potential, which provides additional circumstances for anisotropic form creation and a variety of elongated nanostructures.[51] Typically, a significant aspect in controlling the shape of nanostructures is the manipulation of thermodynamically and kinetically regulated growth regimes.[52]

3.5. SEM Surface Texture. The SEM picture of produced CdO nanorods is depicted in Figure 5. CdO was discovered in several spots at different magnifications, creating many scattered nanorods. The nanorods measured 0.75−1 m in length and 200 nm in diameter, demonstrating the morphology of nanorod array development. Cadmium salt combines with hydroxyl and amide groups along chitosan in water to generate hydrated cadmium ions $n[Cd(H_2O)p]^{2+}$, which are then transformed to cadmium hydroxide ($[Cdn(OH)_2n]$) in the solid form via step-wise coordination of −OH ion and pursuing condensation of −OH linked to individual Cd ions. However, under specific conditions, cadmium hydroxide can be converted into CdO via dehydration, as follows:

$$Cd(OH)_2 + \text{chitosan} \rightarrow CdO + H_2O \quad (2)$$

When certain rods were generated from a dense cluster of nucleation sites, the crystals grew laterally, resulting in basal aggregation formations. When one rod hits another pre-existing rod during growth, it sometimes tends to skip the current structure, resulting in interpenetrative growth between numerous rods.[40] The EDX spectrum was used to analyze the chemical constituents of the CdO nanorods, as depicted in Figure 5d. The hybrid materials have some elemental peaks at 0.51 and 3.21 keV due to the presence of oxygen (O) and cadmium (Cd), respectively.

3.6. XPS Analysis. XPS was used to characterize the as-prepared CdO nanorod to evaluate its surface elemental composition and chemical states. The core-level spectra of C 1s, O 1s, and Cd 3d without further impurities are presented in Figure 6 after being captured and deconvoluted using Avantage software. The spectra were all energy-adjusted using the adventitious carbon binding energy, 284.5 eV. The XPS survey spectra of a CdO nanorod seen in Figure 6a reveal the two primary elements, Cd and O, demonstrating the successful synthesis of CdO. Carbon traces were also found in the survey spectrum. The carbon peak usually arises with a binding energy of approximately 284.5 eV (Figure 6b), generally obtained from the chitosan structure's carbon backbone and the XPS instrument due to calibration. Based on deconvolution analysis, Cd 3d has a concentration of 21.1%, while O 1s and C 1s have an atomic percent of 44.83 and 34.07%, respectively. Figure 6d depicts a typical core-level spectrum of Cd (3d), comprising the Cd 3d5/2 and Cd 3d3/2 spin-orbit constituents with 405.0 and 411.7 eV binding energies, respectively. It is consistent with those reported in refs 53, 54. The Cd (3d) binding energy is ascribed to Cd^{2+} bonding, suggesting the CdO single phase and the absence of CdO_2 or $CaCO_3$ secondary phases. This result is consistent with the XRD results.

3.7. CV Studies. Figure 7 reveals the CV plots of designed electrodes AC and AC@CdO nanorods at ranges between 10 and 100 mV s^{-1}. Both electrodes presented a large surface area by CV curves, revealing excellent electrochemical activity. The determining specific surface area for CdO nanorods was 35.43 m^2/g, probably higher than that published CdO and/or mixed with other metal oxides prepared by different routes.[45,55,56] Both electrodes maintained the CV curve's shape despite the high scan rate of 100 mV s^{-1}, suggesting superior material stability and fast electron transfer in the electrode. By looking at the area under the curve for both fabricated electrodes, we will notice the superiority of the nanoelectrode (AC@CdO) at the expense of its counterpart (AC), which has a clear indication of its superiority in the C_{sp}. Using the law of calculating the specific capacitance (C_{sp}) by measuring CV, the C_{sp} was estimated to be 71.5 for the AC electrode and 120 F g^{-1} for the AC@CdO electrode at 10 mV s^{-1}(Figure 7d).

3.8. GCD Studies. GCD curves were recorded for AC, and AC@CdO electrodes have a similar triangular shape, as shown in Figure 8, with the lowest voltage drop (IR drop) in the

https://doi.org/10.1021/acsomega.3c02261
ACS Omega 2023, 8, 35682−35692

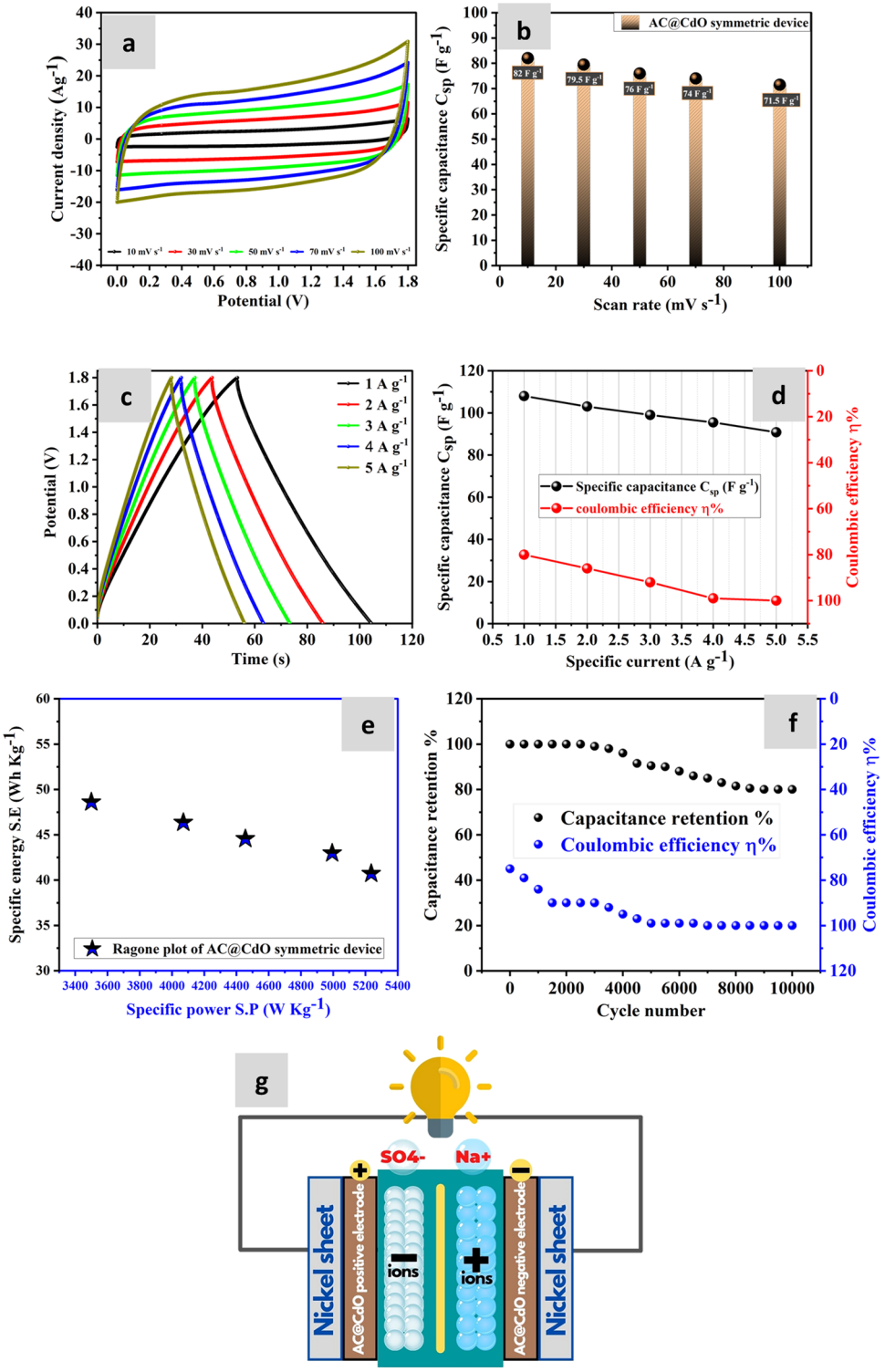

Figure 11. (a) CV curves of the AC@CdO//AC@CdO symmetric supercapacitor device, (b) C_{sp}, (c) GCD curves for the symmetric supercapacitor cell, (d) C_{sp} and coulombic efficiency at specific currents from 1−5 A g^{-1}, (e) Ragone plot, (f) capacitance retention vs coulombic efficiency with cycle number at 5 A g^{-1}, and (g) schematic design in 2D of the symmetric AC@CdO//AC@CdO cell.

potential window range of 0−1 V. A broader discharge curve for the AC@CdO nanoelectrode was produced than the activated carbon electrode, revealing a better C_{sp} for the nanoelectrode that matches the CV results. Figure 8c compares the charging and discharging curves at 0.5 A g^{-1} for both electrodes AC and AC@CdO, which displays the superiority of the nanoelectrode in terms of the large discharge time, demonstrating the remarkable distinction of the nanoelectrode (AC@CdO) in discharge time thus superior in the C_{sp} to its electrode (AC). According to Figure 8d, the electrodes (AC and AC@CdO) have C_{sp} of 105 and 320 F g^{-1} at 0.5 A g^{-1} and 61 and 176 F g^{-1} at 4.5 A g^{-1}. The C_{sp} of the AC@CdO electrode is greater than that of the commercial AC electrode about three times at 0.5 A g^{-1}. Figure 8e shows the coulombic

https://doi.org/10.1021/acsomega.3c02261
ACS Omega 2023, 8, 35682−35692

efficiency (η%) for AC and AC@CdO electrodes which was 75 and 76% at the beginning of the range of specific currents (0.5 A g^{-1}) and 100% at the end of the range of particular currents (4.5 A g^{-1}).

3.9. EIS Studies. Figure 9a shows the EIS curves within a frequency range of 0.01 to 100 kHz. Studying the conductivity properties of materials using the EIS was addressed. As is common knowledge, the higher the separation efficiency and the better the ability of electron transmission, the lower the resistance and interface resistance. The two variables utilized to express the conductivity of the materials used to create the electrode are equivalent series resistance (ESR), whose value of 3.05 Ω for the nanoelectrode (AC@CdO) is still lower than the value of the AC electrode (3.9 Ω), and the charge transfer resistance (R_{ct}). As seen in Figure 9b, the nanoelectrode semicircle is smaller than the AC electrode, reflecting its strong conductivity and lower R_{ct}. Table 2 illustrates the factor for characterizing the AC electrode and AC@CdO nanomaterial electrode in 1 M Na_2SO_4 with (0−1 V) of the potential window.

3.10. Cycle Life Test. At 2.5 A g^{-1} of a specific current, the cycle stability for both electrodes was investigated. According to the results (Figure 10a), 100% of the capacitance retention can be maintained for both electrodes after 10,000 cycles, indicating high cycle stability and no appreciable shape change in the charge−discharge curves in a neutral aqueous solution of Na_2SO_4.

3.11. AC@CdO//AC@CdO Symmetric Supercapacitor Cell. The two-electrode system used to investigate the CV curves for the symmetric AC@CdO//AC@CdO supercapacitor cell is displayed in Figure 11. With weak reversible humps and a quasi-rectangular shape, the CV curves of symmetric cells show outstanding electrochemical behavior. The symmetric cell's CV curves (Figure 11a) offer a range of potential windows (1−1.8 V) and scan rates from 10 to 100 mV s^{-1}. The symmetric AC@CdO//AC@CdO cell displays a specific capacitance value of 82, 79.5, 76, 74, and 71.5 F g^{-1} at scan rates of 10, 30, 50, 70, and 100 mV s^{-1}. This means the CV efficiency descended from 100% at 10 mV s^{-1} to reach 87.2% at 100 mV s^{-1}, as shown in Figure 11b. The symmetric cell GCD curves are measured at different specific currents within 1 and 5 A g^{-1}, which are depicted in Figure 11c. Discharge curves can be used to determine the specific capacitances at various current densities. The symmetric AC@CdO//AC@CdO cell (Figure 11d) delivers 108 F g^{-1} of specific capacitance with coulombic efficiency (η%) of 80% at 1 A g^{-1} and retains 84.26% of that capacitance (91 F g^{-1}) even at 5 A g^{-1} with 100% of coulombic efficiency, showing its higher rate capabilities. Ragone plots' x-axis (specific power) and y-axis (specific energy) are significant indicators to evaluate the practical applications of supercapacitors. The Ragone plot of the symmetric cell in 1 M Na_2SO_4 electrolyte is depicted in Figure 11e. This cell could deliver 48.6 Wh kg^{-1} of specific energy at 3499.2 W kg^{-1} of specific power and retain 40.7 Wh kg^{-1} at 5236 W kg^{-1}. Continuous GCD tests were used to evaluate the symmetric cell's cycling life. According to Figure 11f, after 10,000 GCD cycles, the capacitance retention and coulombic efficiency are 100 and 75%, respectively, and continue to hold at 80 and 100% of the starting values. Figure 11g shows a schematic design in 2D of the symmetric AC@CdO// AC@CdO cell.

4. CONCLUSIONS

In conclusion, this study presented the benign fabrication of nanomaterial CdO nanorods via an abundant biopolymeric chitosan structure under a hydrothermal approach. The CdO nanorods arise as the primary unsubstituted $-NH_2$ of chitosan interacts with the Cd-salt surface at higher temperatures. The electrochemical characteristics of the nanomaterial CdO nanorod were compared with those of the activated carbon material. The high specific capacitance of AC@CdO nanoelectrodes was 320 F g^{-1}, three-fold that of ordinary AC electrodes. Furthermore, after 10,000 GCD cycles, both electrodes had superior capacitance retention with 100% of their initial value at 2.5 A g^{-1}. After the two electrodes were tested, the symmetric supercapacitor cell using AC and CdO nanorods was manufactured with extreme precision. After 10,000 cycles, the symmetrical cell stability achieved 80% capacitance retention and 100% coulombic efficiency. This indicates the potential of fabricated AC@CdO//AC@CdO cell use in energy storage applications.

AUTHOR INFORMATION

Corresponding Author

Kamel R. Shoueir − *Institute of Nanoscience & Nanotechnology, Kafrelsheikh University, Kafrelsheikh 33516, Egypt;* orcid.org/0000-0001-7994-559X; Email: kameltag@yahoo.com

Authors

Rania A. Elmanfaloty − *Department of Electrical and Computer Engineering, Faculty of Engineering, King Abdulaziz University, Jeddah 21589, Kingdom of Saudi Arabia; Department of Electronics and Communications Engineering, Alexandria Higher Institute of Engineering and Technology, Alexandria 21311, Egypt*

Bedir Yousif − *Electrical Engineering Department, Faculty of Engineering, Kafrelsheikh University, Kafrelsheikh 33516, Egypt; Electrical Engineering Department, Faculty of Engineering and Information Technology, Onaizah Colleges, Onaizah, Al Qassim 51911, Saudi Arabia*

Complete contact information is available at: https://pubs.acs.org/10.1021/acsomega.3c02261

Notes

The authors declare no competing financial interest.

ACKNOWLEDGMENTS

The Deanship of Scientific Research (DSR) at King Abdulaziz University (KAU), Jeddah, Saudi Arabia, has funded this project under grant no (G: 366-144-1443).

REFERENCES

(1) Al Jahdaly, B. A.; Abu-Rayyan, A.; Taher, M. M.; Shoueir, K. Phytosynthesis of Co_3O_4 nanoparticles as the high energy storage material of an activated carbon/Co_3O_4 symmetric supercapacitor device with excellent cyclic stability based on a Na_2SO_4 aqueous electrolyte. *ACS Omega* **2022**, *7*, 23673−23684.

(2) Maher, M.; Hassan, S.; Shoueir, K.; Yousif, B.; Abo-Elsoud, M. E. A. Activated carbon electrode with promising specific capacitance based on potassium bromide redox additive electrolyte for supercapacitor application. *J. Mater. Res. Technol.* **2021**, *11*, 1232−1244.

(3) Majumdar, D.; Mandal, M.; Bhattacharya, S. K. Journey from supercapacitors to supercapatteries: recent advancements in electrochemical energy storage systems. *Emergent Mater.* **2020**, *3*, 347−367.

https://doi.org/10.1021/acsomega.3c02261
ACS Omega 2023, 8, 35682−35692

(4) Suberu, M. Y.; Mustafa, M. W.; Bashir, N. Energy storage systems for renewable energy power sector integration and mitigation of intermittency. *Renew. Sustain. Energy Rev.* **2014**, *35*, 499−514.
(5) Lin, X.; Salari, M.; Arava, L. M. R.; Ajayan, P. M.; Grinstaff, M. W. High temperature electrical energy storage: advances, challenges, and frontiers. *Chem. Soc. Rev.* **2016**, *45*, 5848−5887.
(6) Chang, P.; Yang, F.; Xie, Q.; Li, T.; Dong, J. 2D porous carbon nanosheet from sulfonated pitch-based graphene quantum dots for high volumetric performance EDLCs. *J. Power Sources* **2020**, *479*, No. 228825.
(7) Ehsani, A.; Heidari, A. A.; Shiri, H. M. Electrochemical pseudocapacitors based on ternary nanocomposite of conductive polymer/graphene/metal oxide: an introduction and review to it in recent studies. *Chem. Rec.* **2019**, *19*, 908−926.
(8) Chen, L.; Wang, J.; Yang, Z.; Zhang, J.; Hou, S.; Hao, C.; Zhang, J. Recent advances in flexible supercapacitors. *J. Solid State Electrochem.* **2022**, *26*, 2627−2658.
(9) Schoetz, T.; Gordon, L. W.; Ivanov, S.; Bund, A.; Mandler, D.; Messinger, R. J. Disentangling Faradaic, Pseudocapacitive, and Capacitive Charge Storage: A Tutorial for the Characterization of Batteries, Supercapacitors, and Hybrid Systems. *Electrochim. Acta* **2022**, *412*, No. 140072.
(10) Lv, H.; Pan, Q.; Song, Y.; Liu, X.-X.; Liu, T. A review on nano−/microstructured materials constructed by electrochemical technologies for supercapacitors. *Nano-Micro Lett.* **2020**, *12*, 118.
(11) Wassel, A. R.; El-Naggar, M. E.; Shoueir, K. Recent advances in polymer/metal/metal oxide hybrid nanostructures for catalytic applications: A review. *J. Environ. Chem. Eng.* **2020**, *8*, No. 104175.
(12) Baig, N.; Kammakakam, I.; Falath, W. Nanomaterials: A review of synthesis methods, properties, recent progress, and challenges. *Mater. Adv.* **2021**, *2*, 1821−1871.
(13) Pourmortazavi, S. M.; Rahimi-Nasrabadi, M.; Karimi, M. S.; Mirsadeghi, S. Evaluation of photocatalytic and supercapacitor potential of nickel tungstate nanoparticles synthesized by electrochemical method. *New J. Chem.* **2018**, *42*, 19934−19944.
(14) Adib, K.; Sohouli, E.; Ghalkhani, M.; Naderi, H. R.; Rezvani, Z.; Rahimi-Nasrabadi, M. Sonochemical synthesis of Ag_2WO_4/RGO-based nanocomposite as a potential material for supercapacitors electrodes. *Ceram. Int.* **2021**, *47*, 14075−14086.
(15) Shi, M.; Zhu, H.; Yang, C.; Xu, J.; Yan, C. Chemical reduction-induced fabrication of graphene hybrid fibers for energy-dense wire-shaped supercapacitors. *Chin. J. Chem. Eng* **2022**, *47*, 1−10.
(16) Abid, N.; Khan, A. M.; Shujait, S.; Chaudhary, K.; Ikram, M.; Imran, M.; Haider, J.; Khan, M.; Khan, Q.; Maqbool, M. Synthesis of nanomaterials using various top-down and bottom-up approaches, influencing factors, advantages, and disadvantages: A review. *Adv. Colloid Interface Sci.* **2022**, *300*, No. 102597.
(17) Nayak, S.; Kittur, A. A.; Nayak, S. Green synthesis of Silver-Zirconia composite using chitosan biopolymer binder for fabrication of electrode materials in supercapattery application for sustainable energy storage. *Curr. Res. Green Sustain. Chem.* **2022**, *5*, No. 100292.
(18) Duan, H.; Wang, D.; Li, Y. Green chemistry for nanoparticle synthesis. *Chem. Soc. Rev.* **2015**, *44*, 5778−5792.
(19) Sasirekha, C.; Arumugam, S.; Muralidharan, G. Green synthesis of ZnO/carbon (ZnO/C) as an electrode material for symmetric supercapacitor devices. *Appl. Surf. Sci.* **2018**, *449*, 521−527.
(20) Ying, S.; Guan, Z.; Ofoegbu, P. C.; Clubb, P.; Rico, C.; He, F.; Hong, J. Green synthesis of nanoparticles: Current developments and limitations. *Environ. Technol. Innov.* **2022**, *26*, No. 102336.
(21) Khan, F.; Jeong, G.-J.; Singh, P.; Tabassum, N.; Mijakovic, I.; Kim, Y.-M. Retrospective analysis of the key molecules involved in the green synthesis of nanoparticles. *Nanoscale* **2022**, *14*, 14824−14857.
(22) Shoueir, K. R.; El-Desouky, N.; Rashad, M. M.; Ahmed, M. K.; Janowska, I.; El-Kemary, M. Chitosan based-nanoparticles and nanocapsules: Overview, physicochemical features, applications of a nanofibrous scaffold, and bioprinting. *Int. J. Biol. Macromol.* **2021**, *167*, 1176−1197.
(23) Dong, Z.; Chen, C.; Wen, K.; Zhao, X.; Guo, X.; Zhou, Z.; Chang, G.; Zhang, Y.; Dong, Y. A freestanding chitin-derived hierarchical nanocomposite for developing electrodes in future supercapacitor industry. *Polymers (Basel)* **2022**, *14*, 195.
(24) Teaima, M. H.; Elasaly, M. K.; Omar, S. A.; El-Nabarawi, M. A.; Shoueir, K. R. Wound healing activities of polyurethane modified chitosan nanofibers loaded with different concentrations of linezolid in an experimental model of diabetes. *J. Drug Deliv. Sci. Technol.* **2022**, *67*, No. 102982.
(25) Asal, H. A.; Shoueir, K. R.; El-Hagrasy, M. A.; Toson, E. A. Controlled synthesis of in-situ gold nanoparticles onto chitosan functionalized PLGA nanoparticles for oral insulin delivery. *Int. J. Biol. Macromol.* **2022**, *209*, 2188−2196.
(26) Pu, L.; Zhang, J.; Jiresse, N. K. L.; Gao, Y.; Zhou, H.; Naik, N.; Gao, P.; Guo, Z. N-doped MXene derived from chitosan for the highly effective electrochemical properties as supercapacitor. *Adv. Compos. Hybrid Mater.* **2022**, *5*, 356−369.
(27) Meng, D.; Wu, C.; Hu, Y.; Jing, Y.; Zhang, X.; Mahmud, S.; Su, S. P.; Zhu, J. Ingenious synthesis of chitosan-based porous carbon supercapacitors with large specific area by a small amount of potassium hydroxide. *J. Energy Storage* **2022**, *51*, No. 104341.
(28) Menazea, A. A.; Ibrahium, H. A.; Awwad, N. S.; Moustapha, M. E.; Farea, M. O.; Bajaber, M. A. Facile synthesis and high-performance dielectric properties of Polyethylene oxide-chitosan-iron oxide nanocomposite for electrical applications. *J. Mater. Res. Technol.* **2022**, *18*, 2273−2281.
(29) El-Shafai, N. M.; Shukry, M.; Sharshir, S. W.; Ramadan, M. S.; Alhadhrami, A.; El-Mehasseb, I. Advanced applications of the nanohybrid membrane of chitosan/nickel oxide for photocatalytic, electro-biosensor, energy storage, and supercapacitors. *J. Energy Storage* **2022**, *50*, No. 104626.
(30) Xi, Y.; Xiao, Z.; Lv, H.; Sun, H.; Zhai, S.; An, Q. Construction of CuO/Cu-nanoflowers loaded on chitosan-derived porous carbon for high energy density supercapacitors. *J. Colloid Interface Sci.* **2023**, *630*, 525−534.
(31) Handayani, M.; Mulyaningsih, Y.; Anggoro, M. A.; Abbas, A.; Setiawan, I.; Triawan, F.; Darsono, N.; Thaha, Y. N.; Kartika, I.; Sunnardianto, G. K. One-pot synthesis of reduced graphene oxide/chitosan/zinc oxide ternary nanocomposites for supercapacitor electrodes with enhanced electrochemical properties. *Mater. Lett.* **2022**, *314*, No. 131846.
(32) Vijeth, H.; Ashokkumar, S. P.; Yesappa, L.; Vandana, M.; Devendrappa, H. Hybrid core-shell nanostructure made of chitosan incorporated polypyrrole nanotubes decorated with NiO for all-solid-state symmetric supercapacitor application. *Electrochim. Acta* **2020**, *354*, No. 136651.
(33) Anthony, L. S.; Vasudevan, M.; Perumal, V.; Ovinis, M.; Raja, P. B.; Edison, T. N. J. I. Bioresource-derived polymer composites for energy storage applications: Brief review. *J. Environ. Chem. Eng.* **2021**, *9*, No. 105832.
(34) Pratheepa, M. I.; Lawrence, M. Synthesis of pure, Cu and Zn doped CdO nanoparticles by co-precipitation method for supercapacitor applications. *Vacuum* **2019**, *162*, 208−213.
(35) Munawar, T.; Nadeem, M. S.; Mukhtar, F.; Manzoor, S.; Ashiq, M. N.; Batool, S.; Hasan, M.; Iqbal, F. Enhanced photocatalytic, antibacterial, and electrochemical properties of CdO-based nanostructures by transition metals co-doping. *Adv. Powder Technol.* **2022**, *33*, No. 103451.
(36) Anwar, N.; Shakoor, A.; Ali, G.; Ahmad, H.; Niaz, N. A.; Seerat-Ul-Arooj; Mahmood, A. Synthesis and electrochemical characterization of polyaniline doped cadmium oxide (PANI-CdO) nanocomposites for supercapacitor applications. *J. Energy Storage* **2022**, *55*, No. 105446.
(37) Henríquez, R.; Mestra-Acosta, A. S.; Muñoz, E.; Grez, P.; Navarrete-Astorga, E.; Dalchiele, E. A. High-performance asymmetric supercapacitor based on $CdCO_3$/CdO/Co_3 O_4 composite supported on Ni foam. *RSC Adv.* **2021**, *11*, 31557−31565.
(38) Divya, K.; Jisha, M. S. Chitosan nanoparticles preparation and applications. *Environ. Chem. Lett.* **2018**, *16*, 101−112.
(39) Pérez, A. G.; González-Martínez, E.; Águila, C. R. D.; González-Martínez, D. A.; Ruiz, G. G.; Artalejo, A. G.; Yee-Madeira, H.

https://doi.org/10.1021/acsomega.3c02261
ACS Omega 2023, 8, 35682−35692

Chitosan-coated magnetic iron oxide nanoparticles for DNA and rhEGF separation. *Colloids Surf. A Physicochem. Eng. Asp.* **2020**, *591*, No. 124500.
(40) Ghoshal, T.; Kar, S.; Chaudhuri, S. Synthesis of nano and micro crystals of Cd $(OH)_2$ and CdO in the shape of hexagonal sheets and rods. *Appl. Surf. Sci.* **2007**, *253*, 7578−7584.
(41) Weingärtner, H.; Franck, E. U. Supercritical water as a solvent. *Angew. Chem., Int. Ed.* **2005**, *44*, 2672−2692.
(42) Wongpreecha, J.; Polpanich, D.; Suteewong, T.; Kaewsaneha, C.; Tangboriboonrat, P. One-pot, large-scale green synthesis of silver nanoparticles-chitosan with enhanced antibacterial activity and low cytotoxicity. *Carbohydr. Polym.* **2018**, *199*, 641−648.
(43) Shoueir, K.; El-Sheshtawy, H.; Misbah, M.; El-Hosainy, H.; El-Mehasseb, I.; El-Kemary, M. Fenton-like nanocatalyst for photo-degradation of methylene blue under visible light activated by hybrid green DNSA@Chitosan@$MnFe_2O_4$. *Carbohydr. Polym.* **2018**, *197*, 17.
(44) Christuraj, P.; Raja, M. D.; Pari, S.; Kumar, G. S.; Shankar, V. U. Synthesis of Mn doped CdO nanoparticles by co-precipitation method for supercapacitor applications. *Mater. Today Proc.* **2022**, *50*, 2679−2682.
(45) Sadhukhan, S.; Ghosh, T. K.; Roy, I.; Rana, D.; Bhattacharyya, A.; Saha, R.; Chattopadhyay, S.; Khatua, S.; Acharya, K.; Chattopadhyay, D. Green synthesis of cadmium oxide decorated reduced graphene oxide nanocomposites and its electrical and antibacterial properties. *Mater. Sci. Eng. C.* **2019**, *99*, 696−709.
(46) Shoueir, K. R. Green microwave synthesis of functionalized chitosan with robust adsorption capacities for Cr (VI) and/or RHB in complex aqueous solutions. *Environ. Sci. Pollut. Res.* **2020**, *27*, 33020.
(47) Rahman, M. M.; Hussain, M. M.; Asiri, A. M. Ultrasensitive and label-free detection of creatine based on CdO nanoparticles: a real sample approach. *New J. Chem.* **2017**, *41*, 6667−6677.
(48) Thovhogi, N.; Park, E.; Manikandan, E.; Maaza, M.; Gurib-Fakim, A. Physical properties of CdO nanoparticles synthesized by green chemistry via Hibiscus Sabdariffa flower extract. *J. Alloys Compd.* **2016**, *655*, 314−320.
(49) Pandey, S.; Son, N.; Kim, S.; Balakrishnan, D.; Kang, M. Locust Bean gum-based hydrogels embedded magnetic iron oxide nano-particles nanocomposite: Advanced materials for environmental and energy applications. *Environ. Res.* **2022**, *214*, No. 114000.
(50) Bradley, J. S.; Tesche, B.; Busser, W.; Maase, M.; Reetz, M. T. Surface spectroscopic study of the stabilization mechanism for shape-selectively synthesized nanostructured transition metal colloids. *J. Am. Chem. Soc.* **2000**, *122*, 4631−4636.
(51) Kumar, S.; Ahmed, B.; Ojha, A. K.; Das, J.; Kumar, A. Facile synthesis of CdO nanorods and exploiting its properties towards supercapacitor electrode materials and low power UV irradiation driven photocatalysis against methylene blue dye. *Mater. Res. Bull.* **2017**, *90*, 224−231.
(52) Peng, Z. A.; Peng, X. Nearly monodisperse and shape-controlled CdSe nanocrystals via alternative routes: nucleation and growth. *J. Am. Chem. Soc.* **2002**, *124*, 3343−3353.
(53) Thema, F. T.; Beukes, P.; Gurib-Fakim, A.; Maaza, M. Green synthesis of Monteponite CdO nanoparticles by Agathosma betulina natural extract. *J. Alloys Compd.* **2015**, *646*, 1043−1048.
(54) Wang, X.; Yang, Y.; Zhang, F.; Tang, J.; Guo, Z. Facile synthesis of Co_3O4/CdO nanospheres as high rate performance super-capacitors. *Mater. Lett.* **2020**, *261*, No. 127141.
(55) Khairy, M.; Ayoub, H. A.; Banks, C. E. Large-scale production of CdO/Cd $(OH)_2$ nanocomposites for non-enzyme sensing and supercapacitor applications. *RSC Adv.* **2018**, *8*, 921−930.
(56) Sivaram, H.; Selvakumar, D.; Alsalme, A.; Alswieleh, A.; Jayavel, R. Enhanced performance of PbO nanoparticles and PbO-CdO and PbO-ZnO nanocomposites for supercapacitor application. *J. Alloys Compd.* **2018**, *731*, 55−63.

https://doi.org/10.1021/acsomega.3c02261
ACS Omega 2023, 8, 35682−35692